IEEE Access
Multidisciplinary | Rapid Review | Open Access Journal

Received March 8, 2019, accepted April 1, 2019, date of publication April 9, 2019, date of current version April 18, 2019.

Digital Object Identifier 10.1109/ACCESS.2019.2909788

Robust Retinal Image Enhancement via Dual-Tree Complex Wavelet Transform and Morphology-Based Method

DONGMING LI[1,2,3], LIJUAN ZHANG[3,4], CHANGMING SUN[3], TINGTING YIN[4], CHEN LIU[2], AND JINHUA YANG[1]

[1]College of Opto-Electronic Engineering, Changchun University of Science and Technology, Changchun 130022, China
[2]School of Information Technology, Jilin Agricultural University, Changchun 130118, China
[3]Data61, CSIRO, Epping, NSW 1710, Australia
[4]College of Computer Science and Engineering, Changchun University of Technology, Changchun 130012, China

Corresponding author: Jinhua Yang (ldm0214@163.com)

This work was supported in part by the National Science Foundation of China under Grant 61806024, and in part by the Scientific and Technological Research Project of the Department of Education in Jilin Province, China, under Grant JJKH20180637KJ.

ABSTRACT Retinal image processing is very important in the field of clinical medicine. As the first step in retinal image processing, image enhancement is essential. Because the details of a retinal image are complex and difficult to enhance, we present a robust retinal image enhancement algorithm via a dual-tree complex wavelet transform (DTCWT) and morphology-based method in this paper. To begin with, we utilize the pre-processing method to the captured retinal images. Then, the DTCWT is applied to decompose the gray retinal image to obtain high-pass subbands and low-pass subbands. Then, a Contourlet-based enhancement method is applied to the high-pass subbands. For the low-pass subbands, we improve the morphology top-hat transform by adding dynamic multi-scale parameters to achieve an equivalent percentage enhancement and at the same time achieve multi-scale transforms in multiple directions. Finally, we develop the inverse DTCWT method to obtain the enhanced retinal image after processing the low-frequency subimages and high-frequency subimages. We compare this approach with enhancement based on the adaptive unsharp masking, histogram equalization, and multi-scale retinex. We present the test results of our algorithm on 440 retinal images from the DRIVE and the STARE databases. The experimental results show that the proposed approach can achieve better results, and might be helpful for vessel segmentation.

INDEX TERMS Retinal image, dual-tree complex wavelet transform, top-hat transform, image enhancement.

I. INTRODUCTION

In the medical field, the visualization of retinal vessel image is important for disease diagnosis and improving the planning and navigation in interventional procedures [1]. For instance, retinal images are widely used to help doctors diagnose many diseases, including diabetes, hypertension, and cardiovascular disease. Due to major reasons like the imaging process and retinal diseases, the obtained retinal images via fundus camera often have poor illumination, low intensity contrast and blur, making it hard to recognize the vascular structure clearly. The useful information of retinal image has been hindered by blur, uneven comparison, and unclear contour [2], [3]. Before making a formal diagnosis on retinal optic disc, macula lutea, and blood vessels, it is necessary to improve retinal image quality [4]. The enhancement of retinal image can make the image processing steps easier and greatly improve the result of feature segmentation. In order to make correct diagnosis, an effective way to overcome those issues is to use some form of vessel-like structure enhancement in retinal images [5].

Image enhancement has been applied to areas of science and engineering, such as computer vision, biomedicine, and astrophotography. Enhancement, followed by segmentation, quantification and modelling of blood vessels in retinal images plays an important role in computer-aided retinopathy diagnosis. Accuracy of the retinal enhancement algorithms (to be reviewed in Section II) have been used to improve

The associate editor coordinating the review of this manuscript and approving it for publication was Wenbing Zhao.

2169-3536 © 2019 IEEE. Translations and content mining are permitted for academic research only.
Personal use is also permitted, but republication/redistribution requires IEEE permission.
See http://www.ieee.org/publications_standards/publications/rights/index.html for more information.

the image quality. In this paper, we present a new method of retinal image enhancement via dual-tree complex wavelet and multi-scale top-hat transforms. Our proposed algorithm studies the retinal image features, and uses the advantages of dual-tree complex wavelet transform (DTCWT) and multi-scale top-hat transforms.

The rest of this paper is organised as follows. In section II, the related works about retinal image enhancement are briefly reviewed. Section III gives a brief overview about our algorithm. Section IV introduces and explains the proposed morphology-based method: improved morphological top-hat transform (IMT-TH). The retinal image enhancement algorithm is applied to real retinal images and the results are presented in Section V. Finally in Section VI we conclude.

II. RELATED WORKS

In the following section, we review existing algorithms for retinal image enhancement. A wide range of retinal image enhancement algorithms have been proposed for many years, and they can be categorized into five groups: Histogram-based methods, Retinex-based methods, Wavelet transform-based methods, Mathematical morphology-based methods, and other methods.

(1) Histogram-based methods [6]–[9] utilize the prior information of blood vessel to equal the histogram distribution. The commonly used method called histogram equalization (HE) [6] helps transforming the gray-level of individual pixels according to histogram, and it is a basic method used for the retinal vessel enhancement. The retinal image enhancement requires more details on complex distribution of blood vessels. Babu and Rajamani presented a contrast enhancement method based on modified histogram equalization (HE) for gray scale image enhancement [7]. To avoid over-enhancement of noise, a contrast limiting procedure is applied between regions, howerver background noise still exists. As the HE method may reduce the local details within different objects, an increasing number of improved HE methods are emerged to improve the local details such as multipeak histogram equalization [10], imprving the visual quality of resonance images using HE [11], and brightness preserving dynamic histogram equalization [12]. However, these are contrast enhancement-based methods that do not perform well as summarized in [7].

(2) Retinex-based methods [13]–[16] belong to image-domain algorithms, have been proposed to enhance the contrast. The idea of retinex was conceived by Land [14] as a model of the lightness and color perception of human vision. Through the years, the modified multi-scale Retinex (MSR) algorithm proposed by Herscovitz and Yadid-Pecht [15] exhibited its superiority for the high-quality enhanced results by removing the illumination. It is also applied to wide dynamic range scenes and points, and improved the global brightness contrast by adjusting the histogram. Moreover, it is unreasonable to simply remove the illumination for the scene of unsmooth depth [17].

(3) Wavelet transform-based methods [18]–[22] have been widely used in medical image processing. Mallat [18] proposed a fast discrete wavelet transform method that has been widely applied in image enhancement field. Fu *et al.* [19] proposed a wavelet-based histogram equalization to enhance sonogram images. The wavelet transform method decomposes input image into high frequency detail and low frequency components at various resolutions. However, wavelet transform has some serious constrains like smoothness edges, exiting noise and poor directional selectively. Some new transforms have been presented to take advantage of wavelet transform. The Contourlet transform [20] and the Dual-Tree Complex Wavelet Transform(DTCWT) [21] are better than Wavelet transform in terms a sparse represent natural images. DTCWT allows perfect reconstruction while still providing the other advantages of complex wavelets [21], [22]. It also has some important additional properties including approximate shift invariance, better directional selectivity in two-dimensional (2-D) with Gabor-like filters, and lower computational complexity [22]. Therefore, it can characterize textures more accurately. In this work, a new algorithm for retinal image enhancement that is based on DTCWT is proposed, because DTCWT can provide approximate shift invariance with a limited redundancy(2^m : 1 for m-dimensional signals) and improve angular resolution(including six oriented subbands,($\pm 15°$, $\pm 45°$, $\pm 75°$)).

(4) Mathematical morphology-based methods [23]–[26] have been widely used for image processing operations and have become the foundation of biomedical computing. Bangham *et al.* [23] presented morphlological scale-space preserving transforms in many dimensions for the analysis of images. Bai *et al.* [24] proposed a novel algorithm for enhance images by using multi scale morphological top-hat transform for image features extracted. Liao *et al.* [25] proposed new method which combines morphological transforms and histogram fitting stretching for retinal vessel enhancement. Moreover, the multi scale theory could be used in mathematical morphology to enhance the useful image details and achieve an efficient performance [26]. Recently, in [27], a multiscale bowler-hat transform method based on mathematical morphology for vessel enhancement is proposed. A major drawback of this method is sensitivity to noise and large computational demand.

(5) Other approaches such as the unsharp masking methods [28]–[31], and Ranklets [32], [33] are proposed for enhancing the image edge and detail information. In [29], Ramponi introduce a cubic unsharp masking method for contrast enhancement. He constructs the well-known unsharp masking(UM) technique, and the proposed method has reduced noise sensitivity. The contrast enhancement of images are introduced in the adaptive unsharp masking (AUM) method [28], which outperforms cubic unsharp masking [29] for accomplishing the dual objectives of avoiding noise amplification as well as excessive overshoot in the detail areas.The AUM method often fails to achieve good tradeoff between details and the naturalness, so it need a

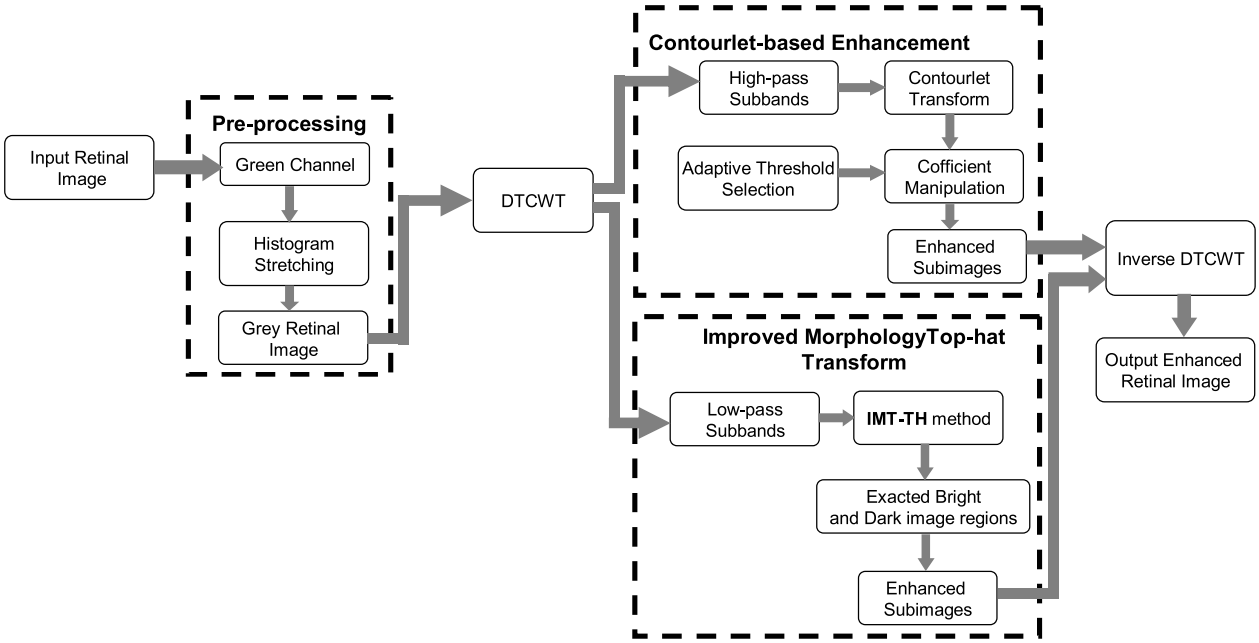

FIGURE 1. The flow chart of our method for retinal image enhancement.

rescaling process to achieve the best result [34]. Smeraldi introduced a new family of rank features,called Ranklets. Ranklets have the ability of the orientation selectivity and the multiscale nature, are used to the classification of feature vectors [32]. Masotti *et al.* [33] proposed false positive reduction using gray-scale invariant ranklet texture features in computer-aided detection.

Many exiting retinal enhancement methods still have substantial issues when faced with variations in constrast, high level of noise, large image size (high computing time), and complexity of parameter space.

III. OUTLINE OF THE PROPSED METHOD

We would like to give an outline of the proposed method. Firstly, the captured retinal images are processed by the pre-processing method. The retinal images acquired with a fundus camera need to transformed from RGB to greyscale. The pre-processing method is based on [20]. For the obtained color retinal image, we extract its green channel, then applying histogram stretching to the grey retinal image. Secondly, the DTCWT is applied. The gray retinal image (basing on the DTCWT method) is decomposed into six high-pass subbands and two low-pass subbands. For high-pass subbands, we use the wavelet-based contourlet transform method for denoising, then get the enhanced high-pass subimages. For low-pass subbands, we use improved morphology top-hat transform method for enhancement, then getting the low-pass subimages. Lastly, the inverse DTCWT method is applied to the obtaind subimages, and the final enhanced retinal image is obtained. The framework of our method is shown in Fig. 1.

The detailed descriptions for each of the steps will be given in the following sections.

IV. METHODOLOGY

In this section, we introduce our novel, dual-tree complex wavelet transform and morphology-based method for retinal image enhancement: the improved morphology top-hat transform.

A. DTCWT FOR THE RETINAL IMAGE

The retinal image is decomposed primarily using the DTCWT [21] over four scales, and each scale produces six high-pass subbands and two low-pass subbands shown in Fig. 2. In Fig. 2, DTCWT customs two distinct trees to represent the wavelet cofficient's real (tree a) and imaginary (tree b) parts, $\downarrow 2$ represents alternate sampling. Let $h_0(n)$, $h_1(n)$ denote the low-pass/high-pass filter pair for the upper filter bank (FB), and let $g_0(n)$, $g_1(n)$ denote the low-pass/high-pass filter pair for the lower FB.

The DTCWT uses analytic filters to perform the wavelet analysis. DTCWT decomposes a signal according to a complex shifted and dilated mother wavelet $\Psi(t)$ and scaling function $\phi(t)$ [22]. The DTCWT is obtained on the basis of the complex wavelet which is defined as

$$\Psi(t) = \Psi_h(t) + j\Psi_g(t) \tag{1}$$

where $j = \sqrt{-1}$, $\Psi_h(t)$ and $\Psi_g(t)$ represent the wavelet's real part and imaginary part, respectively, and they are wavelet basis functions.

In order to reduce shift sensitivity and to carry out perfect reconstruction, the DTCWT is obtained from traditional discrete wavelet transform step by step. On the issue of shift sensitivity, two conditions must be satisfied between the low-pass filter and the high-pass filter. Firstly, they need to

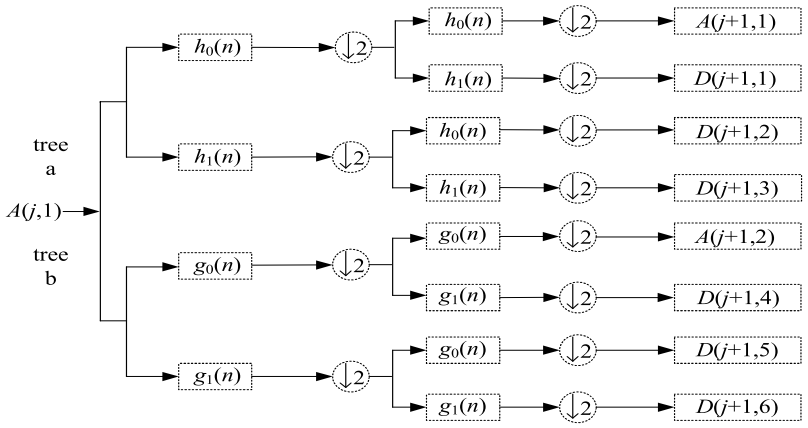

FIGURE 2. Diagram of 2D dual-tree complex wavelet transform.

constitute a Hilbert transform pair, and the phase difference is 90°. Signals in a Hilbert transform pair relate to each other via the Hilbert transform, and the modulus of the complex signal (so $\sqrt{signal_1^2 + signal_2^2}$) is invariant, but the amplitude of the combined to signals (as a complex signal) is invariant. Also the invariance to shifts only holds locally and approximately in the theory of CWT. According to the Selesnick theorem, the two low-pass filters ($h_0(n)$, $g_0(n)$) should satisfy a very simple property: one of them should be approximately a half-sample shift of the other [22], that is

$$g_0(n) \approx h_0(n - 0.5) \tag{2}$$

In this case, the corresponding wavelet basis $\Psi_h(t)$ and $\Psi_g(t)$ and can form an approximate Hilbert transform pair, that is

$$\Psi_g(t) \approx \tilde{H}\{\Psi_h(t)\} \tag{3}$$

Since $g_0(n)$ and $h_0(n)$ are defined only on integers, this statement is somewhat informal. However, we can make the statement rigorous using Fourier transforms. In [22], it is shown that if

$$G_0(e^{j\omega}) = e^{-j0.5\omega} H_0(e^{j\omega}) \tag{4}$$

Then $\Psi_g(t) = \tilde{H}\{\Psi_h(t)\}$.

Here we define the analysis filters as $h_0(n)$, $h_1(n)$, defining the synthesis filters by $\tilde{h}_0(n)$ and $\tilde{h}_1(n)$. Assuming that the analysis and symthesis filters are real finite impulse response (FIR) filters, the perfect reconstruction condition can be satisfied if $h_0(n) \times \tilde{h}_0(n)$ is a low-pass half band filter [22]. Specifically, if we define the product filter

$$p(n) = h_0(n) * \tilde{h}_0(n) \tag{5}$$

where $*$ represents discrete-time convolution. Then for perfect reconstruction (with a delay of n_0 samples), it is necessary that

$$p(2n + n_0) = \delta(n) = \begin{cases} 1, & n = 0 \\ 0, & n \neq 0 \end{cases} \tag{6}$$

where the two high-pass filters are given by

$$h_1(n) = (-1)^{n+d} \tilde{h}_0(n - d) \tag{7}$$

$$\tilde{h}_1(n) = -(-1)^{n+d} h_0(n + d) \tag{8}$$

where d is an even (odd) integer when n_0 is an odd (or even) integer.

The analysis wavelet $\Psi(t)$ associated with these filters is given by

$$\Psi(t) = \sqrt{2} \sum_n h_1(n) \phi(2t - n) \tag{9}$$

where $\phi(t)$ is called the scaling function and is given implicitly by [22]

$$\phi(t) = \sqrt{2} \sum_n h_0(n) \phi(2t - n) \tag{10}$$

Eq. (10), which is called the dilation equation, is an important equation in the theory of wavelet bases and has been studied extensively since the advent of wavelet transforms [35].

To explain how the DTCWT produces oriented wavelets, consider the 2-D wavelet

$$\Psi(x, y) = \Psi(x)\Psi(y) \tag{11}$$

Associated with the row-column implementation of the wavelet transform, where $\Psi(x)$ is a complex wavelet given by Eq. (1) which is $\Psi(x) = \Psi_h(x) + j\Psi_g(x)$, we can obtain the expression for $\Psi(x, y)$ which is

$$\begin{aligned} \Psi(x, y) &= (\Psi_h(x) + j\Psi_g(x))(\Psi_h(y) + j\Psi_g(y)) \\ &= \Psi_h(x)\Psi_h(y) - \Psi_g(x)\Psi_g(y) \\ &\quad + j(\Psi_g(x)\Psi_h(y) + \Psi_h(x)\Psi_g(y)) \end{aligned} \tag{12}$$

The 2D DTCWT produces six high-pass subbands as well as two lowpass subbands at each level of decomposition. As a result, wavelets are oriented in ($\pm 15°$, $\pm 45°$, $\pm 75°$) directions and captures image information in those directions.

B. WBCT-BASED ENHANCEMENT FOR HIGH-PASS SUBBANDS

In [36], we proposed a wavelet-based contourlet transform (WBCT) method to image denoising. This method is implemented through combining with BayesShrink theory to estimate the threshold and then improving the adaptive method of selecting threshold, finally obtaining the optimal threshold. The WBCT transform coefficients of different decomposition scales and different direction to select the adaptive optimal threshold to achieve denoising. In this paper, for the high-pass subbands of the retinal image after docomposition(based on the 2D DTCWT), we use the WBCT method for enhancement and obtain the enhanced subimages. The WBCT method is summarized in [36].

C. OUR PROPOSED MORPHOLOGY-BASED ENHANCEMENT METHOD FOR LOW-PASS SUBBANDS

1) MATHEMATICAL MORPHOLOGY

Mathematical morphology has been widely used for image processing [26], and it belongs to a branch of mathematics. Most of the morphology operations are defined based on two basic operations: dilation and erosion. Let $f(x, y)$ denote a grayscale image with the size of $M \times N$, and $B(u, v)$ represent a structuring element. The dilation and the erosion of $f(x, y)$ by $B(u, v)$, denoted by $f \oplus B$ and $f \ominus B$ respectively. Based on dilation and erosion, opening and closing of $f(x, y)$ by $B(u, v)$, represented by $f \circ B$ and $f \bullet B$ respectively. Applying opening and closing operations, the top-hat transform of $f(x, y)$ by $B(u, v)$ are defined as

$$WTH(x, y) = f(x, y) - f \circ B(x, y) \tag{13}$$

$$BTH(x, y) = f \bullet B(x, y) - f(x, y) \tag{14}$$

where $WTH(x, y)$ is called the classical white top-hat transform, which is usually used to extract bright image regions, and $BTH(x, y)$ is the classical black top-hat transform, which is used to extract dim image regions.

Therefore, one way for retinal image enhancement through contrast enhancement based on the traditional top-hat transform is adding the bright image regions and subtracting the dim image regions from the original image as follows:

$$f_{en} = f + f_w - f_b \tag{15}$$

where f_{en} is the final enhanced image, f is the original image, f_w is the extracted bright image regions, and f_b is the extracted dim image regions.

The traditional top-hat transform refers to white top-hat transform, and its purpose is to enhance shadow details of the gray image and to highlight foreground objects. Fig. 3 is the white top-hat transform on retinal images for image enhancement. Fig. 3(a) is the original retinal images from the STARE database [37] (top) and the DRIVE database [38] (bottom). The white top-hat transform on Fig. 3(a) are shown in Fig. 3(b), and the enhancement results based on Fig. 3(b) are shown in Fig. 3(c).

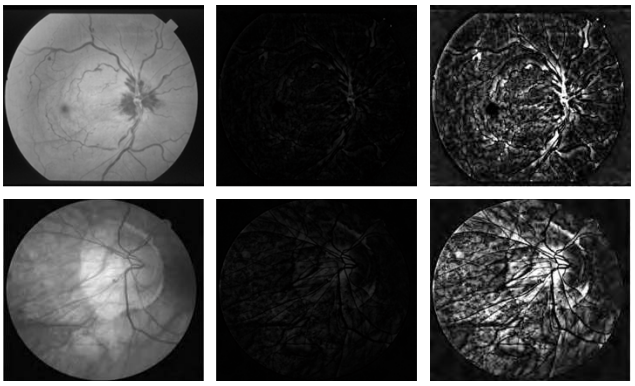

FIGURE 3. Example results of the white top-hat transform on the STARE database and the DRIVE database. (a) From top to bottom: the original retinal images of the STARE database and the DRIVE database, respectively; (b) Results from the white top-hat transform; (c) Results from the enhancement processing.

From these experimental results, we can see that the white top-hat transform is not effective for retinal images with complex background, uneven gray scale image intensities, and detailed textures.

2) IMPROVED MORPHOLOGY TOP-HAT TRANSFORM

In order to effectively enhance retinal image details, enhance image edge information, and improve the retinal image quality, we present an improved morphology top-hat transform (IMT-TH) for low-pass subbands.

The definitions of $WTH(x, y)$ and $BTH(x, y)$ indicate that, because only one structuring element B is used in the classical top-hat transform, the different information from the regions of interest and its surrounding regions could not be effectively used for image enhancement [24]. To avoid the unsatisfactory enhanced result caused by the inappropriate structuring element, we utilize multi-scale top-hat transform in this paper to enhance the low-pass subbands of the decomposed retinal image.

Since the bright and dark regions require different structuring elements, and different detail regions also need to dynamically change the structuring elements, all of those will undoubtedly increase the complexity of the top-hat transform. Therefore we define a structuring element sequence $B = \{B_0, \cdots, B_i, \cdots, B_n\}$, where B_0 is the initial selected structuring element, $B_i = \underbrace{B_0 \oplus B_0 \cdots \oplus B_0}_{i \quad times}$ and $1 \le i \le n$. That is, the ith scale B_i is derived from the expansion transform of the initially selected structuring element B_0.

The top-hat transform of the retinal image f by structuring element B_i can be defined as

$$\begin{cases} WTH_i(x, y) = f - f \circ B_i \\ BTH_i(x, y) = f \bullet B_i - f \end{cases} \tag{16}$$

In the retinal image enhancement process, in addition to the image region on each scale needing enhancement, the details between scales also need to be enhanced. The details

between the scales include details from both bright and dark regions, and the multi-scale image details can be denoted by $DWTH_i(x, y)$ and $DBTH_i(x, y)$, which are

$$\begin{cases} DWTH_i(x, y) &= WTH_{i+1}(x, y) - WTH_i(x, y) \\ DBTH_i(x, y) &= BTH_{i+1}(x, y) - BTH_i(x, y) \end{cases} \tag{17}$$

In Eq. (15), the extracted bright image regions f_w contains the bright details $WTH_i(x, y)$ on the ith scale and the bright details $DWTH_i(x, y)$ between different scales. The extracted dark image regions f_b contains the dark details $BTH_i(x, y)$ on the ith scale and the dark details $DBTH_i(x, y)$ between different scales.

In retinal images, the interest regions are usually bright or dark image regions. The white improved top-hat transform ($WTH_i(x, y)$) could extract bright image regions. In the result of white improved top-hat transform, the gray values of the extracted bright image regions are larger than other regions. Then, the multi-scale bright image regions between different scales should have the largest gray values. Similarly, the final dark image regions could be constructed through the extracted multi-scale dark image regions. Therefore, the optimal bright and dark image regions denoted by f_w^R and f_b^R, are defined as

$$\begin{cases} f_w^R = \max\limits_{1 \le i \le n} \{WTH_i(x, y)\} \\ f_b^R = \max\limits_{1 \le i \le n} \{BTH_i(x, y)\} \end{cases} \tag{18}$$

where f_w^R is the final bright image regions, f_b^R is the final dark image regions.

Similarly, we also define the optimal bright and dark image details which are denoted by f_w^D and f_b^D, respectively, that is

$$\begin{cases} f_w^D = \max\limits_{1 \le i \le n} \{DWTH_i(x, y)\} \\ f_b^D = \max\limits_{1 \le i \le n} \{DBTH_i(x, y)\} \end{cases} \tag{19}$$

where f_w^D is the final bright image details between different scales, f_b^D is the final dark image details between different scales.

According to Eq. (18) and Eq. (19), we can obtain all the extracted multi-scale bright and dark image regions, that is

$$\begin{cases} f_w = f_w^R + f_w^D \\ f_b = f_b^R + f_b^D \end{cases} \tag{20}$$

In order to achieve the same proportion enhancement, and to obtain a better enhancement result, we use the scale control parameter λ. In the image enhancement process, the white top-hat transform and the black top-hat transform should be set the same λ to achieve the same proportion enhancement. This method is the IMT-TH method, which can be performed by

$$\begin{aligned} f_{en} &= f + \lambda_i(f_w - f_b) \\ &= f + \lambda_i((f_w^R + f_w^D) - (f_b^R + f_b^D)) \end{aligned} \tag{21}$$

where λ_i is a scale control parameter at each scale for the retinal image. When eyes are completely adapted to illumination conditions, we can obtain a response curve which is similar to an S type by testing the light stimulation of neurons. According to this feature, we use the image edge gradient information to construct the scale control parameter. So, λ_i can be defined as

$$\lambda_i = Sigmoid(E(x, y)) \tag{22}$$

where $E(x, y)$ is an image edge detection operator, function $Sigmoid()$ is a common S type function, that is

$$Sigmoid(x) = \frac{1}{1 + e^{-x}} \tag{23}$$

According to morphological operation, we develop a morphology algorithm for image edge extraction. Then, according to the morphological dilation, we define the image edge detection operator E_d, as

$$E_d(x, y) = f \oplus B_i(x, y) - f \tag{24}$$

Similarly, we also define the image edge detection operator E_e according to the morphological erosion, as

$$E_e(x, y) = f - f \ominus B_i(x, y) \tag{25}$$

The image edge detection operator $G(x, y)$ based on the multi-structural dilation- erosion type (also known as the morphological gradient) is

$$G(x, y) = f \oplus B_i(x, y) - f \ominus B_i(x, y) \tag{26}$$

Blurred edges will be added to the image by using edge detection based on the dilation method, while some details will be lost to image edge by using edge detection based on an erosion method. In order to reduce the blurred image edge and retain more image edge details for obtaining the ideal image edge, we correct the above edge detection operator, as

$$\begin{cases} E_{max}(x, y) = \max\{E_d(x, y), E_e(x, y), G(x, y)\} \\ E_{min}(x, y) = \min\{E_d(x, y), E_e(x, y), G(x, y)\} \\ E_{dec}(x, y) = E_{max}(x, y) - E_{min}(x, y) \end{cases} \tag{27}$$

So the new image edge detection operator $E(x, y)$ is defined as

$$E(x, y) = E_d(x, y) + kE_{dec}(x, y) \tag{28}$$

where k is an enhancement ratio. Then put $E(x, y)$ into Eq. (22), we can obtain the scale control parameter λ_i.

The corrected edge detection operator $E(x, y)$ is now obtained, and the fuzziness of image edge detection will be reduced. On this basis, the multi-scale top-hat transform method can improve the anti-noise ability and detect image edges more efficiently. The results of our IMT-TH algorithm on the STARE [37] and the DRIVE [38] databases are shown in Fig. 4. Fig. 4(a) is the original gray images from the STARE database (top) and the DRIVE database (bottom); Fig. 4(b) is the white top-hat transformation for Fig. 4(a); Fig. 4(c) is the dark top-hat transformation for Fig. 4(a); Fig. 4(d) is

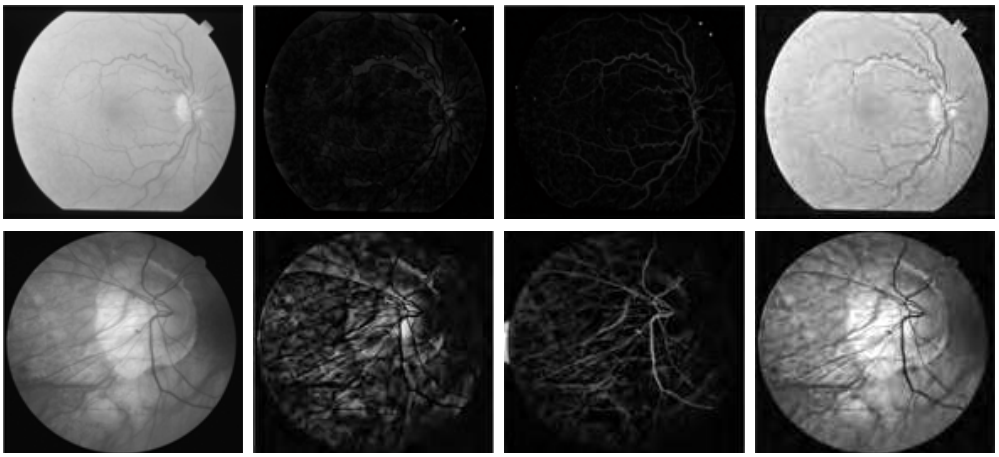

FIGURE 4. Results of the IMT-TH on the STARE database and the DRIVE database. (a) From top to bottom: the original retinal images of the STARE database and the DRIVE database, respectively; (b)-(c) The corresponding transform of (a) obtained from white top-hat transform, and dark top-hat transform; (d) Results of our IMT-TH algorithm.

the results for enhancing retinal images combining the white top-hat transformation with the dark top-hat transformation, which is based on our IMT-TH algorithm. Based on the results, a trade-off between the structuring element B_0 and the parameter n for better performances is observed, and the parameters are set at B_0 with the size of 3×3, $n = 12$ that were selected experimentally for visually acceptable results.

It can be seen from Fig. 4 that the IMT-TH method can enhance retinal images effectively. This method combines the advantages of both the white top-hat transform and the dark top-hat transform, and has a great improvement in clarity and visual contrast.

D. IMPLEMENTATION

The specific implementation steps for our algorithm are summarized in Algorithm 1.

V. EXPERIMENTAL RESULTS AND DISCUSSION

We evaluate the performance of the propsed algorithm through applications to retinal images from two publicly available retinal image databases as samples: the DRIVE database, and the STARE database. We compare our results with three other methods: the adaptive unsharp masking (AUM) method [28], the histogram equalization (HE) method [6], and the multi-scale Retinex (MSR) method [15]. The reason we choose these three methods is that AUM method is good at noise removal. HE method is a classic Histogram-based method for constrast and line feature enhancements. MSR method has very good performance in terms of the high-quality enhanced results and restoration. In the following sub-sections, we define the image quality assessment method. Then we compare our method with those three methods and give the statistical results.

The poor-quality retinal images do not allow an accurate medical diagnosis, and it is inconvenient for a patient to return to a medical center to repeat the fundus photography exam. In this paper, our approach could help improve the the overall accuracy, sensitivity, or specificity in automated diagnosis, retinal blood segmentation [39], and image classification [40] tasks. The purpose of retinal image enhancement is to enhance contrast between foreground and background, which is proposed by ophthalmologist to facilitate their clinical diagnosis. In [39], the authors first employed a set of retinal image enhancement steps to correct the nonuniform illumination of retinal images and to improve vessel constrast, then they used convolutional neural network (CNN) method for retinal blood vessel segmentation. Retinal disease detection by using computer-aided diagnosis form fundus image has emerged as a new mehtod. In [40], they investigated multi-categorical classification of deep learning for automated diagnosis by using fundus photograph (which has been preprocessed by using retinal image enhancement method). Our study will provide proper way to ophthalmologists who continue researching on a better quality retinal image in terms for clinical use.

A. EXPERIMENTS SETTING

In this study, all the experiments are implemented in MATLAB R2012b and conducted on a 64-bit personal computer with Intel i7-7500U CPU at 2.7GHz, 8.0 GB RAM, and Microsoft Windows 10 operating system. Similar to most of the retinal image enhancement methods, the proposed approach is evaluated on two well estabilished public databases: the DRIVE database [38] and the STARE database [37]. These datasets have been chosen because of their availability.

Algorithm 1 Steps for our proposed enhancement algorithm.

- **Step 1**: Pre-processing. Input the color retinal image and exact its green channel. Then, apply historgram stretching to obtain the grey retinal image [20];
- **Step 2**: Perform DTCWT operation. The grey retinal image $f(x, y)$ is decomposed into six high-pass subbands $(D(j+1, i), i = 1, 2, \cdots, 6)$ as well as two low-pass subbands $(A(j+1, 1), A(j+1, 2))$, with the algorithm described in Section IV-A;
- **Step 3**: Obtain the enhanced low-pass retinal image f_{en}. According to the method described in Section IV-C, the two low-pass subbands $(A(j+1, 1), A(j+1, 2))$ are processed and obtain the low-frequency subimages, according to Eq. (21), with our IMT-TH method, and obtained the enhanced low-pass subimages;
- **Step 4**: Obtain the high-frequency enhanced retinal image f_{hde}. For the high-pass sub-bands D after DTCWT decomposition, we use our proposed WBCT-based enhacement method [36], then obtain the denoising image f_{hde}:
  (1) Calculate the Contourlet transform of six high-pass subbands $(D(j+1, i), i = 1, 2, \cdots, 6)$. Then, we get a set of coeffiecients $C_{p,q}$ of the scale p and direction q for each subband, and correspond to a given resolution level;
  (2) Calculate the noise standard deviation $\hat{\sigma}_v^2$;
  (3) The coefficients of subbands are processed consulting the adaptive threshold selection method (the detail process can see [36]);
  (4) WBCT inverse transform of the modified coefficient $\hat{C}_{p,q}$ is used to obtain the enhanced high-pass subimages;
- **Step 5**: the inverse DTCWT method is applied to the obtaind subimages, and the final enhanced retinal image $\hat{f}_{en}(x, y)$ is obtained.

There are several parameters in our method: the length for the structure element B_0, and the enhancement ratio k. The selection for structuring element B_0 mainly considers the isotropic requirement in the algorithm. The parameter k determines the ratio of the bright and dark detail features in the retinal image, which directly affects the retinal image detail performance and visual effects. In general, the range of the parameter k is within [0.5, 1], and it can also be flexibly chosen according to the specific application target and the need to enhance detail features. The parameter n for better performances is observed, and the maximum value is 16.

B. SUBJECTIVE EVALUATION

The subjective evaluation on the retinal image enhancement quality is in terms of good visibility and image contrast. In our experiments, retinal images from the DRIVE and the STARE databases were tested to evaluate the proposed enhancement algorithm. We use the same parameters on all retinal images. The parameters are set at $k = 0.5$, $B_0 = 3 \times 3$, and $n = 7$ which are selected experimentally for visually acceptable results in this paper, and we use the same size and format on all retinal images. Fig. 5 shows enhanced examples of four randomly selected blurry retinal images which are from the DRIVE database are illustrated for comparing our proposed method with the AUM method, the HE method, the MSR method. In Fig. 5, the first column is the original retinal images. The AUM's results in the second column have nonuniform background grey distribution and over-enhanced textures in the dim region. The HE's results in the third column have much brighter background making parts of the vessels invisible in the enhanced image than they should be. The MSR's results in the fourth column have optic disc and parts of vessel information loss. As show in the last column, our method enhances the constrast between vessels and background successfully, has more naturally enhanced images with improved visibility, clear details, high clarity.

For a better comparison and quantitative analysis, we then tested the four methods on ninety retinal images in the STARE database [37] and observed the results. We compare the quality of the enhanced retinal images from our proposed IMT-TH method with the related works developed on the basis of the AUM method [28], the HE method [6], and the MSR method [15], and the comparison on the enhancement results are shown in Fig. 6. As shown in Fig. 6(a), the four original input retinal images are randomly selected from the STARE database [37]. As shown in Fig. 6(b), the results of the AUM method have low contrast and insufficient brightness around the main blood vessels, which usually lead to decrease the ability of vessel enhance accuracy. As shown in Fig. 6(c), the results of the HE method have some distortion especially in the optic disc regions because some details of bright region are over enhanced. As shown in Fig. 6(d), the results of the MSR method have image contour distortion and little enhancement on the optic disc and the macula due to the incorrect scales estimations. As shown in Fig. 6(e) for the results of our proposed IMT-TH method, we can see that our work increases the visibility adaptively while respecting the brightness for the optic disc and the surrounding main blood vessels, which clearly shows its superiority over the other three methods. The visual effects of the main features such as blood vessel, optic disc, and macula are significantly improved. In particular, the brightness of the optic disc and the surrounding main blood vessels has greatly improved. All of these are beneficial for blood vessel segmentation, retinal vessel extraction, and image contour preserving.

C. OBJECTIVE EVALUATION

While a visual inspection can give some information regarding the effectiveness of the retinal enhancement methods, a form of quantitative validation is required. To solve this problem, a widely used blind assessmet method (Mean Value, Standard Deviation, and Image Shannon Information Entropy [41]) based on the property of human visual

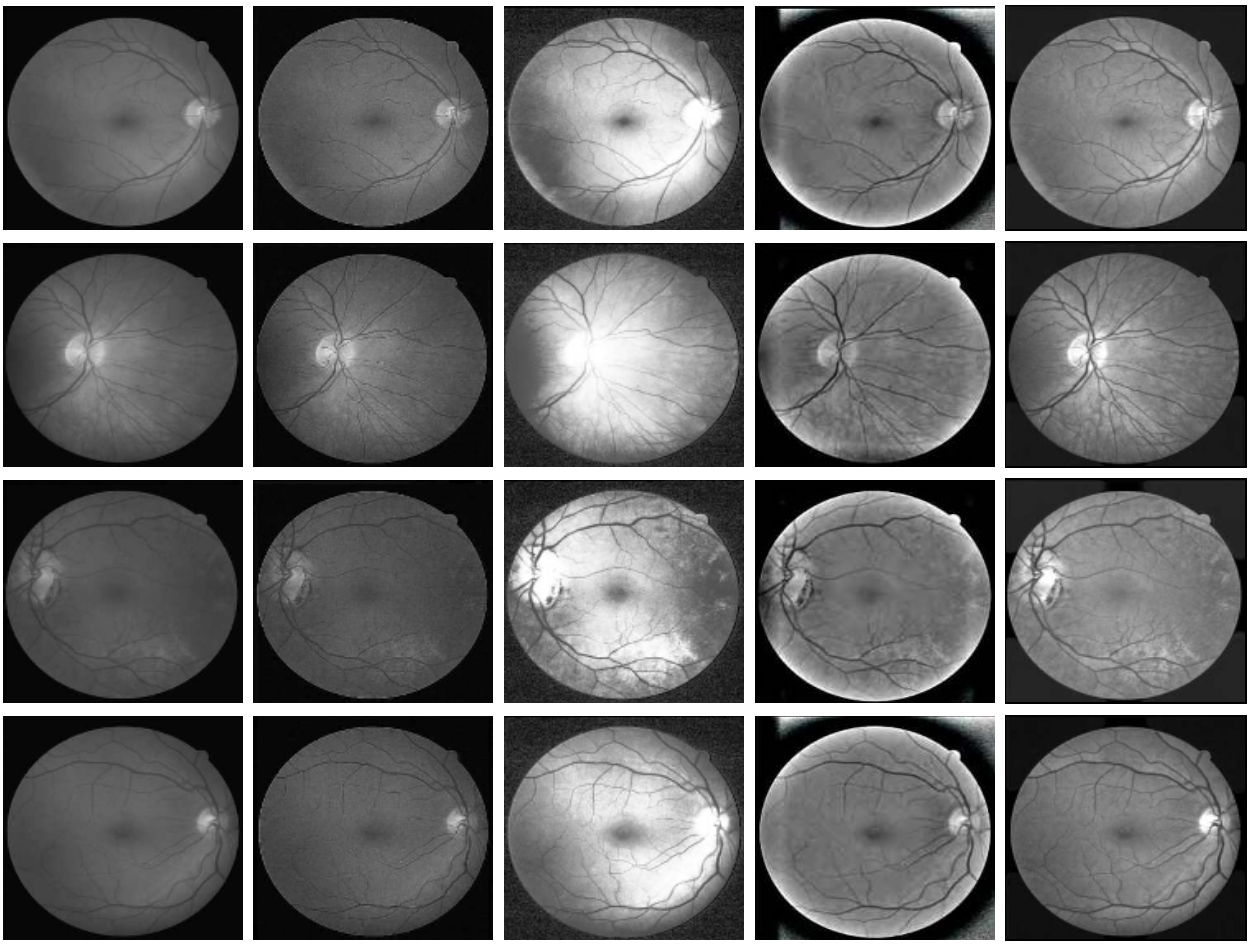

FIGURE 5. The original retinal images and the comparison results of the enhanced retinal images based on four algorithms on the DRIVE database. (a) From top to bottom: Retinal images on the DRIVE database; (b) obtained using the AUM algorithm; (c) obtained using the HE algorithm; (d) obtained using the MSR algorithm; (e) obtained using our algorithm.

system is adopted to objectively evaluate the state-of-the-art enhancement methods and our proposed method. The E_{MV} is defined as

$$E_{MV} = \frac{1}{MN}\sum_{x=1}^{M}\sum_{y=1}^{N}\hat{f}_{en}(x,y) \tag{29}$$

where (x, y) is the pixel coordinate of image, $\hat{f}_{en}(x, y)$ represents the enhanced retinal image, and M and N represent the width and height of the image $\hat{f}_{en}(x, y)$. E_{MV} is the average value of image pixels, which reflects the brightness of the image. A large E_{MV} value indicates that a high brightness of enhanced image is obtained.

E_{SD} refers to the discrete degree between the image pixel gray value and the mean value E_{MV}. A larger E_{SD} value indicates that the gray-scale in the image is dispersed and a better enhanced image quality is obtained. The E_{SD} is defined as

$$E_{SD} = \sqrt{\frac{1}{MN}\sum_{x=1}^{M}\sum_{y=1}^{N}(\hat{f}_{en}(x,y) - E_{MV})^2} \tag{30}$$

The difinition of Shannon information entropy for a specific event is simply to take the (natural) logarithm of its probability. For the image information, the information entropy is defined by Shannon as [41],

$$E_{IIE} = -\sum_{x=1}^{M}\sum_{y=1}^{N} p_{x,y}\log_2(p_{x,y}) \tag{31}$$

It is required that $\sum_{x=1}^{M}\sum_{y=1}^{N} p_{x,y} = 1$. E_{IIE} represents the average number of bits in the image gray level set and the unit of E_{IIE} is bits/pixel. E_{IIE} also describes the average information amount of the image source. E_{IIE} can be used to compare the image information differences between the different images. $p_{x,y}$ refers to the probability of a certain intensity occuring in the image ($\hat{f}_{en}(x, y)$), and it can be express as

$$p_{x,y} = \frac{\hat{f}_{en}(x,y)}{M \times N} \tag{32}$$

In general, the larger the value of E_{IIE} is, the more abundant the information is and a better enhanced image quality is obtained.

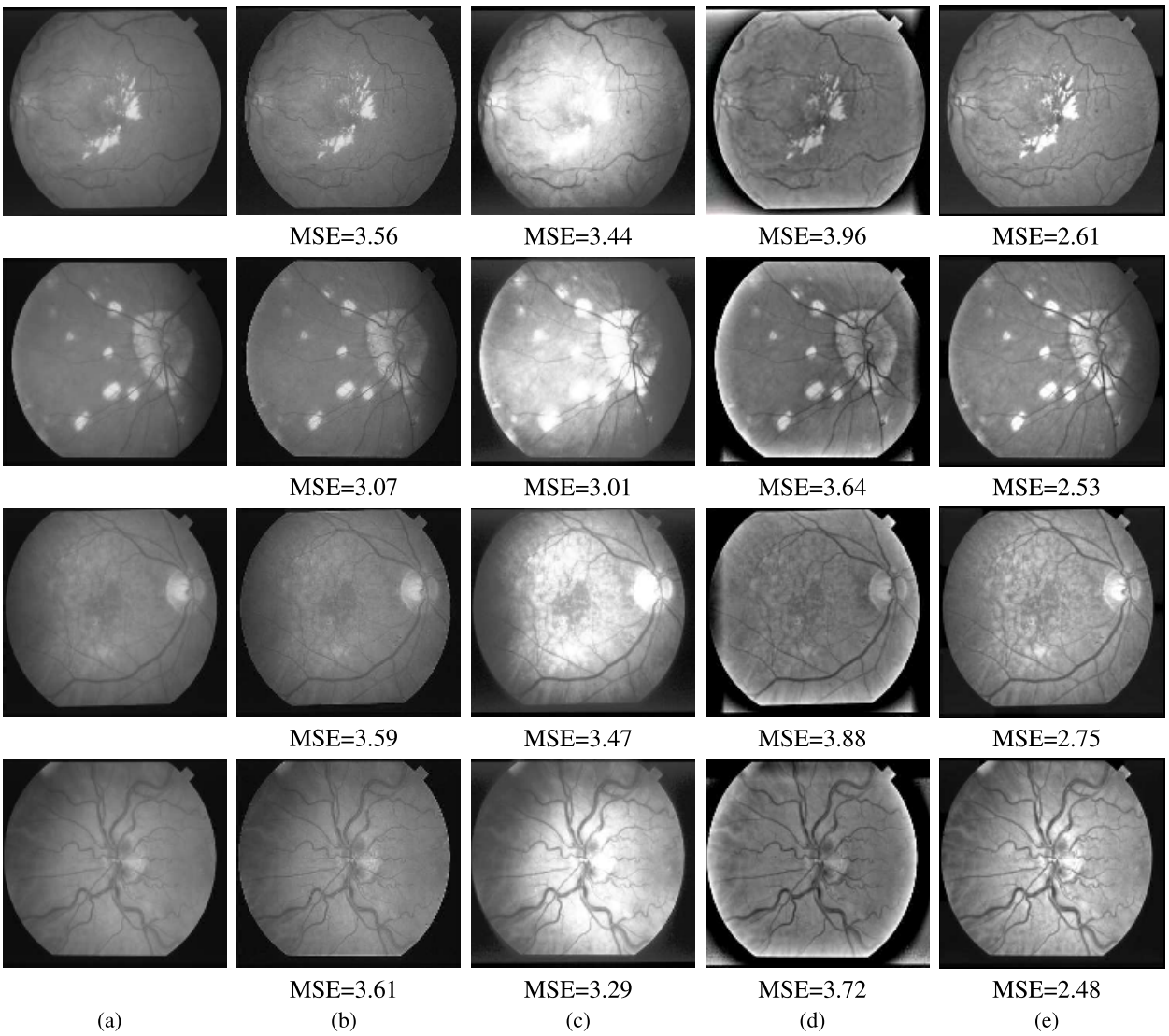

FIGURE 6. Quantitative comparison of enhancement results on the STARE database. (a) input retinal images on the STARE database; (b) by the AUM algorithm; (c) by the HE algorithm; (d) by the MSR algorithm; (e) by our algorithm.

In order to prevent the uncertainty of single retinal image measurement, we randomly select 15 retinal images in the DRIVE database. In order to verify our algorithm, we compare our algorithm with the original retinal image and two other algorithms (the HE, and AUM algorithms) for the retinal images in the DRIVE database. Because the MSR method is not effective, and the image distortion from the algorithm is severe, it will not be included in the following index comparison. The objective evaluation criteria for the experimental results are measured by E_{MV}, E_{SD}, and E_{IIE}, which are shown in Table 1. Based on the combination of the results on E_{MV} in Table 1 with the illustrations given in Fig. 5, the HE and the AUM methods with the lower values of E_{MV} have produced uneven illuminance around the main blood vessels. Our proposed method have improved the brightness of the vessel lead to visible details more than the other methods. Based on the combination of the results on E_{SD} in Table 1 with the illustrations given in Fig. 5, the HE method with the highest E_{SD} value has produced nonuniform background grey distribution leading to parts of the vessels invisible. The AUM method with the lowest E_{SD} value has produced over-enhanced textures in dim region. Our proposed method with the second higher E_{SD} value can enhance the contrast better than the HE, and the AUM methods. Based on the combination of the results on E_{IIE} in Table 1 with the illustrations given in Fig. 5, the HE and the AUM methods have the lower values of E_{IIE} because of the over-enhanced contrast. Our IMT-TH method has improved the image clarity more than the other methods.

In order to show the reliability of our proposed method, it is compared with other image quality index such as the mean square error (MSE) [42]. The MSE is calculated as

$$MSE = \frac{1}{MN}\sum_{x=1}^{M}\sum_{y=1}^{N}(\hat{f}_{en}(x,y) - f(x,y))^2 \tag{33}$$

where $f(x, y)$ is the original retinal image.

TABLE 1. Comparison results on E_{MV}, E_{SD}, and E_{IIE} of different enhancement algorithms on the drive database.

Retinal Image Names	Evaluation Criterions	Original Retinal Image	HE	AUM	Our Algorithm
img01	E_{MV}	83.2071	89.5148	83.8654	**110.7796**
	E_{SD}	52.7117	**64.9571**	53.5592	59.6486
	E_{IIE}	5.6152	5.6763	6.3790	**6.4694**
img02	E_{MV}	99.9982	87.8555	100.0760	**120.7621**
	E_{SD}	64.0253	63.0014	64.6521	**65.3391**
	E_{IIE}	5.7303	5.5326	6.3973	**6.4578**
img03	E_{MV}	64.0059	90.7993	64.0645	**93.5726**
	E_{SD}	39.3232	**62.9090**	39.6996	50.9283
	E_{IIE}	5.2909	6.0365	6.0583	**6.3471**
img04	E_{MV}	83.8988	91.7695	84.7313	**99.0774**
	E_{SD}	55.5316	**62.9090**	56.6652	59.0816
	E_{IIE}	6.1315	6.0365	6.7331	**6.7418**
img05	E_{MV}	77.5596	85.5484	77.6908	**101.4045**
	E_{SD}	48.9181	**62.3145**	49.2750	54.7387
	E_{IIE}	5.5006	5.3978	6.2152	**6.2698**
img06	E_{MV}	79.6353	89.2156	80.5116	**113.6095**
	E_{SD}	50.1028	**66.3758**	51.4518	60.6193
	E_{IIE}	5.4694	5.6704	6.2518	**6.5014**
img07	E_{MV}	88.0413	95.5417	88.9123	**105.9922**
	E_{SD}	57.7802	63.5859	63.5859	**67.2614**
	E_{IIE}	6.1287	6.1422	6.7343	**6.8558**
img08	E_{MV}	83.7366	87.0945	84.0839	**99.1244**
	E_{SD}	54.0284	**63.6272**	54.5028	56.2256
	E_{IIE}	5.7357	5.5125	**6.4066**	6.3586
img09	E_{MV}	95.7008	94.4369	96.4744	**105.7807**
	E_{SD}	60.6614	**65.5754**	61.3723	64.5794
	E_{IIE}	5.4940	5.8540	**6.2299**	6.2254
img10	E_{MV}	69.4501	94.6050	69.8740	**99.6164**
	E_{SD}	44.3607	**62.6219**	44.8807	52.9136
	E_{IIE}	5.6747	6.1764	6.3722	**6.4491**
img11	E_{MV}	95.2530	87.2255	95.0126	**109.0693**
	E_{SD}	62.4455	62.0698	63.0228	**63.6907**
	E_{IIE}	6.0979	5.5382	**6.7130**	6.6437
img12	E_{MV}	86.9224	91.3038	88.3648	**105.2011**
	E_{SD}	55.0938	**66.0565**	56.3354	63.3221
	E_{IIE}	5.5681	5.7999	**6.3499**	6.3391
img13	E_{MV}	89.1217	95.6900	90.0684	**100.7208**
	E_{SD}	57.2281	**64.1385**	58.1386	62.1285
	E_{IIE}	5.7752	6.0806	6.4963	**6.5649**
img14	E_{MV}	89.0614	90.9987	90.6489	**112.7131**
	E_{SD}	56.1271	**65.9292**	57.5085	64.8462
	E_{IIE}	5.7215	5.6773	6.4391	**6.6096**
img15	E_{MV}	66.8999	84.3228	67.5794	**90.6939**
	E_{SD}	45.4781	**61.3554**	46.2908	52.8838
	E_{IIE}	6.0851	5.6039	6.6915	**6.7519**
Average values	E_{MV}	83.4994	90.3948	84.1305	**104.5411**
	E_{SD}	53.5877	**62.8284**	54.3902	59.8805
	E_{IIE}	5.7345	5.7801	6.4311	**6.5057**

The MSE is calculated between the enhanced results for each method and the original retinal image for quantitative comparison. The lower MSE represents that the image enhancement result is closer to the ground truth while a higher MSE means that the enhancement effect is unsatisfactory. So a smaller MSE demonstrates a better results. We show

TABLE 2. Average mse for four methods.

Methods	AUM method	HE method	MSR method	Our method
Average MSE(%)	3.46	3.30	3.80	2.59

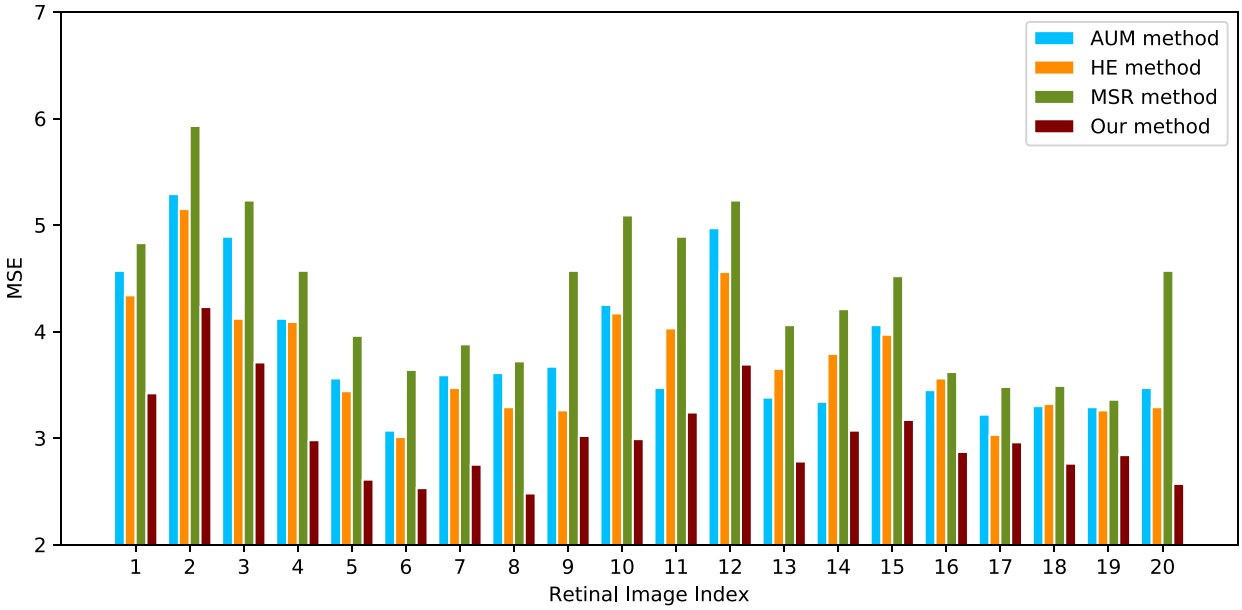

FIGURE 7. The histogram of MSE for all the images using four methods. It can be observed that the error of our method is smaller than that of the other three methods.

four enhancement examples in Fig. 6 and the average MSE values for all the test data in Table 2. Moreover, we plot the histogram of MSE for the fifteen randomly selected enhancement retinal images on the STARE database in Fig. 7. The enhancement results of our proposed method have lowest MSEs and have the most similar structures to the ground truth compared with the AUM, the HE, and the MSR methods. The effectiveness of our IMT-TH image enhancement method is verified objectively.

Our method takes about 23 s with an Intel Core i7 2.7GHz processor and 8 GB RAM using MATLAB R2012b to process a 300 $\times$ 300 pixel retinal image shown in the fourth row in Fig 6, while the AUM method takes about 14 s, the HE method takes 11 s and the MSR takes 17 s to process this image. Although the proposed method is slightly larger time-computating, the better performance makes it more applicable in real applications.

VI. CONCLUSION

In this paper, we propose a new enhancement method for retinal image based on our DTCWT strategy and mathematical morphology which is used for effective high-pass subbands denoising and low-pass subbands enhancement. There are two main contributions in this paper. The first contribution is the introduction of DTCWT strategy to decompose the gray retinal image into high-pass subbands and low-pass subbands, which helps complete decomposition and reconstruction, and preserves more image details as well. The second contribution is the proposal of our IMT-TH method for processing the low-pass subbands enhancement, which can adaptively achieve an equivalent percentage enhancement and multi scale transform in multiple directions. Our method greatly improves the retinal image enhanced results in comparing with the AUM method, the HE method, and MSR method. Meanwhile, both subjective and objective experimental results indicate that our proposed method has a much better enhancement results in feature restoration, image contrast, and high clarity. The proposed method is significant that can be applied to the preprocessing for segmentation, feature extraction, and image classification. Future work will focus on detecting the exact contours of lesions for the retinal images.

ACKNOWLEDGMENT

The authors would like to thank for DRIVE database and the STARE databases. They also would like to thank the anonymous reviewers for their helpful and constructive comments.

REFERENCES

[1] B. Chen, C. Yang, Z. Shao, T. Tong, and L. Luo, "Blood vessel enhancement via multi-dictionary and sparse coding: Application to retinal vessel enhancing," *Neurocomputing*, vol. 200, pp. 110–117, Aug. 2016.

[2] A. Lazareva, P. Liatsis, and F. G. Rauscher, "Hessian-LoG filtering for enhancement and detection of photoreceptor cells in adaptive optics retinal images," *J. Opt. Soc. Amer. A*, vol. 33, no. 1, pp. 84–94, 2016.
[3] X. Fei, J. Zhao, H. Zhao, D. Yun, and Y. Zhang, "Deblurring adaptive optics retinal images using deep convolutional neural networks," *Biomed. Opt. Express*, vol. 8, no. 12, pp. 5675–5687, 2017.
[4] H. Chang, K. Michael, W. Wang, and T. Zeng, "Retinex image enhancement via a learned dictionary," *Opt. Eng.*, vol. 54, no. 1, 2015, Art. no. 013107. doi: 10.1117/1.OE.54.1.013107.
[5] Y. Zhao, L. Rada, K. Chen, S. P. Harding, and Y. Zheng, "Automated vessel segmentation using infinite perimeter active contour model with hybrid region information with application to retinal images," *IEEE Trans. Med. Imag.*, vol. 34, no. 9, pp. 1797–1807, Sep. 2015.
[6] S. M. Pizer *et al.*, "Adaptive histogram equalization and its variations," *Comput. Vis., Graph., Image Process.*, vol. 39, no. 3, pp. 355–368, 1987.
[7] P. Babu and V. Rajamani, "Contrast enhancement using real coded genetic algorithm based modified histogram equalization for gray scale images," *Int. J. Imag. Syst. Technol.*, vol. 25, no. 1, pp. 24–32, Mar. 2015.
[8] S. Anand and S. Gayathri, "Mammogram image enhancement by two-stage adaptive histogram equalization," *Optik*, vol. 126, no. 21, pp. 3150–3152, Nov. 2015.
[9] A. F. M. Raffei, H. Asmuni, R. Hassan, and R. M. Othman, "A low lighting or contrast ratio visible iris recognition using iso-contrast limited adaptive histogram equalization," *Knowl., Based Syst.*, vol. 74, pp. 40–48, Jan. 2015.
[10] K. Wongsritong, K. Kittayaruasiriwat, F. Cheevasuvit, K. Dejhan, and A. Somboonkaew, "Contrast enhancement using multipeak histogram equalization with brightness preserving," in *Proc. IEEE. APCCAS IEEE Asia–Pacific Conf. Circuits Syst. Microelectron. Integrating Syst.*, Nov. 1998, pp. 455–458.
[11] N. S. P. Kong and H. Ibrahim, "Improving the visual quality of abdominal magnetic resonance images using histogram equalization," in *Proc. Int. Conf. Inf. Technol. Appl. Biomed.*, May 2008, pp. 138–139.
[12] N. S. P. Kong and H. Ibrahim, "Color image enhancement using brightness preserving dynamic histogram equalization," *IEEE Trans. Consum. Electron.*, vol. 54, no. 4, pp. 1962–1968, Nov. 2008.
[13] J. H. Jang, S. D. Kim, and J. B. Ra, "Enhancement of optical remote sensing images by subband-decomposed multiscale retinex with hybrid intensity transfer function," *IEEE Geosci. Remote Sens. Lett.*, vol. 8, no. 5, pp. 983–987, Sep. 2011.
[14] E. Land, "An alternative technique for the computation of the designator in the retinex theory of color vision," *Proc. Nat. Acad. Sci. USA*, vol. 83, no. 10, pp. 3078–3080, 1986.
[15] M. Herscovitz and Y. O. Yadid-Pecht, "A modified Multi Scale Retinex algorithm with an improved global impression of brightness for wide dynamic range pictures," *Mach. Vis. Appl.*, vol. 15, no. 4, pp. 220–228, Oct. 2004.
[16] L. Meylan and S. Susstrunk, "High dynamic range image rendering with a Retinex-based adaptive filter," *IEEE Trans. Image Process.*, vol. 15, no. 9, pp. 2820–2830, Sep. 2006.
[17] B. Li, S. Wang, and Y. Geng, "Image enhancement based on Retinex and lightness decomposition," in *Proc. 18th IEEE Int. Conf. Image Process.*, Brussels, Belgium, Sep. 2011, pp. 3417–3420.
[18] S. G. Mallat, "A theory for multiresolution signal decomposition: The wavelet representation," *IEEE Trans. Pattern Anal. Mach. Intell.*, vol. 11, no. 7, pp. 674–693, Jul. 1989.
[19] J. C. Fu, J. W. Chai, and S. T. C. Wong, "Wavelet-based enhancement for detection of left ventricular myocardial boundaries in magnetic resonance images," *Magn. Reson. Imag.*, vol. 18, no. 9, pp. 1135–1141, Nov. 2000.
[20] P. Feng, Y. Pan, B. Wei, W. Jin, and D. Mi, "Enhancing retinal image by the Contourlet transform," *Pattern Recognit. Lett.*, vol. 28, no. 4, pp. 516–522, Mar. 2007.
[21] N. Kingsbury, "The dual-tree complex wavelet transform: A new technique for shift invariance and directional filters," in *Proc. IEEE Digit. Signal Process. Workshop*, Aug. 1998, pp. 319–322.
[22] I. W. Selesnick, R. G. Baraniuk, and N. C. Kingsbury, "The dual-tree complex wavelet transform," *IEEE Signal Process. Mag.*, vol. 22, no. 6, pp. 123–151, Nov. 2005.
[23] J. A. Bangham, R. W. Harvey, P. D. Ling, and R. V. Aldridge, "Morphological scale-space preserving transforms in many dimensions," *J. Electron. Imaging*, vol. 5, no. 3, pp. 283–299, 1996.
[24] X. Bai, F. Zhou, and B. Xue, "Image enhancement using multi scale image features extracted by top-hat transform," *Opt. Laser Technol.*, vol. 44, no. 2, pp. 328–336, Mar. 2012.
[25] M. Liao, Y.-Q. Zhao, X.-H. Wang, and P.-H. Dai, "Retinal vessel enhancement based on multi-scale top-hat transformation and histogram fitting stretching," *Opt. Laser Technol.*, vol. 58, pp. 56–62, Jun. 2014.
[26] X. Bai, F. Zhou, and B. Xue, "Fusion of infrared and visual images through region extraction by using multi scale center-surround top-hat transform," *Opt. Express*, vol. 19, no. 9, pp. 8444–8457, 2011.
[27] C. Sazak, C. Nelson, and B. Obara, "The multiscale bowler-hat transform for blood vessel enhancement in retinal images," *Pattern Recognit.*, vol. 88, pp. 739–750, Apr. 2019. doi: 10.1016/j.patcog.2018.10.011.
[28] A. Polesel, G. Ramponi, and V. J. Mathews, "Image enhancement via adaptive unsharp masking," *IEEE Trans. Image Process.*, vol. 9, no. 3, pp. 505–510, Mar. 2000.
[29] G. Ramponi, "A cubic unsharp masking technique for contrast enhancement," *Signal Process.*, vol. 67, no. 2, pp. 211–222, Jun. 1998.
[30] T. Luft, C. Colditz, and O. Deussen, "Image enhancement by unsharp masking the depth buffer," *Acm Trans. Graph.*, vol. 25, no. 3, pp. 1206–1213, Jul. 2006.
[31] L. Lu, Y. Gaobo, and X. Ming, "Anti-forensics for unsharp masking sharpening in digital images," *Int. J. Digit. Crime Forensics*, vol. 5, no. 3, pp. 53–65, Jul. 2013.
[32] F. Smeraldi, "Ranklets: Orientation selective non-parametric features applied to face detection," *Object Recognit. Supported User Interact. Service Robots*, Aug. 2002, pp. 379–382.
[33] M. Masotti, N. Lanconelli, and R. Campanini, "Computer-aided mass detection in mammography: False positive reduction via gray-scale invariant ranklet texture features," *Med. Phys.*, vol. 36, no. 2, pp. 311–316, 2009.
[34] S. Wang, J. Zheng, H.-M. Hu, and B. Li, "Naturalness preserved enhancement algorithm for non-uniform illumination images," *IEEE Trans. Image Process.*, vol. 22, no. 9, pp. 3538–3548, Sep. 2013.
[35] G. Strang, "Wavelets and dilation equations: A brief introduction," *Siam Rev.*, vol. 31, no. 4, pp. 614–627, 1989.
[36] D.-M. Li, L.-J. Zhang, J.-H. Yang, and W. Su, "Research on wavelet-based contourlet transform algorithm for adaptive optics image denoising," *Optik*, vol. 127, no. 12, pp. 5029–5034, Jun. 2016.
[37] A. D. Hoover, V. Kouznetsova, and M. Goldbaum, "Locating blood vessels in retinal images by piecewise threshold probing of a matched filter response," *IEEE Trans. Med. Imag.*, vol. 19, no. 3, pp. 203–210, Mar. 2000.
[38] J. Staal, M. D. Abramoff, M. Niemeijer, M. A. Viergever, and B. V. Ginneken, "Ridge based vessel segmentation in color images of the retina," *IEEE Trans. Med. Imag.*, vol. 23, no. 4, pp. 501–509, Apr. 2004.
[39] S. Wang, Y. Yin, G. Cao, B. Wei, Y. Zheng, and G. Yang, "Hierarchical retinal blood vessel segmentation based on feature and ensemble learning," *Neurocomputing*, vol. 149, pp. 708–717, Feb. 2015.
[40] J. Y. Choi, T. K. Yoo, J. G. Seo, J. Kwak, T. T. Um, and T. H. Rim, "Multi-categorical deep learning neural network to classify retinal images: A pilot study employing small database," *PLoS One*, vol. 12, no. 11, Nov. 2017, Art. no. e0187336.
[41] C. E. Shannon, "A mathematical theory of communication," *Bell Syst. Tech. J.*, vol. 27, no. 3, pp. 379–423, 1948.
[42] R. Su, C. Sun, C. Zhang, and T. D. Pham, "A new method for linear feature and junction enhancement in 2D images based on morphological operation, oriented anisotropic Gaussian function and Hessian information," *Pattern Recognit.*, vol. 47, no. 10, pp. 3193–3208, 2014.

DONGMING LI received the M.E. degree from the Changchun University of Technology, Changchun, China, in 2006, where he is currently pursuing the Ph.D. degree with the College of Opto-Electronic Engineering. He then joined Jilin Agricultural University, Changchun, where he is currently a Professor carrying out teaching and research on projects. He was a Visiting Scholar with CSIRO, Australia, from 2016 to 2017. His current research interests include computer vision, image analysis, and pattern recognition.

LIJUAN ZHANG received the M.E. and Ph.D. degrees from the Changchun University of Science and Technology, Changchun, China, in 2004 and 2015, respectively. She was a Visiting Scholar with CSIRO, Australia, from 2016 to 2017. She is currently a Professor with the College of Computer Science and Engineering, Changchun University of Technology. Her research interests include image restoration, computer vision, and image analysis.

CHANGMING SUN received the Ph.D. degree in computer vision from Imperial College London, London, U.K., in 1992. He then joined CSIRO, Sydney, Australia, where he is currently a Principal Research Scientist carrying out research and working on applied projects. His current research interests include computer vision, image analysis, and pattern recognition. He has served on the program/organizing committees of various international conferences. He is an Associate Editor of the *EURASIP Journal on Image and Video Processing*.

TINGTING YIN received the B.E. degree in computer application from the Huazhong University of Science and Technology, in 2015, and the M.E. degree from the Changchun University of Technology, in 2017. Her current research interests include computer vision and image analysis.

CHEN LIU is currently pursuing the B.E. degree in Internet of Things engineering with the School of Information Technology, Jilin Agricultural University, Changchun, China, in 2016. His current research interests include machine learning and image analysis.

JINHUA YANG received the B.E. degree from Xian University, in 1994, the M.E. degree from the Beijing Institute of Technology University, in 1997, and the Ph.D. degree from the Changchun University of Science and Technology, in 2001. Since 2001, he has been undertaking postdoctoral researches with The University of Tokyo. He is currently a Professor and a Ph.D. Supervisor of science field is photoelectric detection technology and quality control. His research interests include artificial intelligence, computer vision, and image processing theory.